RESULTS AND INTERPRETATIONS OF THE SPIN STRUCTURE EXPERIMENTS AT SLAC

Yury G. Kolomensky
California Institute of Technology
Pasadena, CA 91125

Representing the E154 and E155 Collaborations

ABSTRACT

In the recent experiments E154 and E155 at SLAC the spin-dependent structure functions g_1^n, g_1^p, and g_1^d of the neutron, proton, and deuteron were measured by scattering longitudinally polarized 48.3 GeV electrons off longitudinally polarized targets. We report on the measurement of g_1^n by E154, and on the preliminary results on g_1^p from E155. The SLAC results provide the most precise determination to date of the polarized structure functions.

We observe relatively large values of g_1^n at low x that call into question the reliability of data extrapolation to $x \to 0$. Such divergent behavior disagrees with predictions of the conventional Regge theory, but is qualitatively explained by perturbative QCD. We perform a Next-to-Leading Order perturbative QCD analysis of the world data on the nucleon spin-dependent structure functions. Using the parameterizations of the helicity-dependent parton distributions obtained in the analysis, we evolve the data to $Q^2 = 5$ GeV^2, determine the first moments of the polarized structure functions of the proton and neutron, and find agreement with the Bjorken sum rule.

1 Introduction

Understanding the structure of the nucleon is one of the most fascinating challenges facing modern physics. Deep-inelastic scattering (DIS) experiments provide perhaps our cleanest window on hadronic structure at large momentum transfer squared Q^2. The original DIS experiments at SLAC[1] built the foundation for the quark-parton model.[2–4] As the precision of the measurements improved, the scaling violations were revealed, and the unpolarized DIS data were used to provide stringent tests of perturbative QCD, measure the strong coupling, and determine the gluon distribution.

While the measurements of the unpolarized structure functions have long reached maturity, studies of the spin structure of the nucleon have only recently come of age. The first polarized deep-inelastic scattering experiments were done at SLAC three decades ago.[5,6] These measurements confirmed the parton model expectations of the large spin asymmetries in the electron-proton scattering at high x, the fraction of nucleon momentum carried by a struck quark. The subsequent measurement of the proton spin structure function g_1^p at higher energies by the EMC Collaboration at CERN[7] revealed that the asymmetries are small at low x. The naive parton model interpretation of their data is that the quarks contribute very little to the proton's spin—in contradiction with quark models. This surprising result, dubbed *the spin crisis* at the time, generated great theoretical and experimental interest.

Since that measurement, much more data have become available from SLAC,[8–10] CERN,[11,12] and DESY.[13] The recent measurements done at SLAC have further improved our knowledge of nucleon structure. In experiment E154,[14] we have measured the structure function g_1^n of the neutron with high precision and over a broad kinematic range. The recent preliminary results from experiment E155 have improved the precision on g_1^p, and the new data on the structure function g_1^d of the deuteron will be available shortly. The latest results, combined with the world spin structure data, have been used[15] to determine the polarized parton distributions and confirm the fundamental Bjorken sum rule.[16]

1.1 Polarized Structure Functions

Our primary concern is with deep-inelastic scattering off polarized targets. Experiments at SLAC and DESY used polarized electrons while experiments at CERN

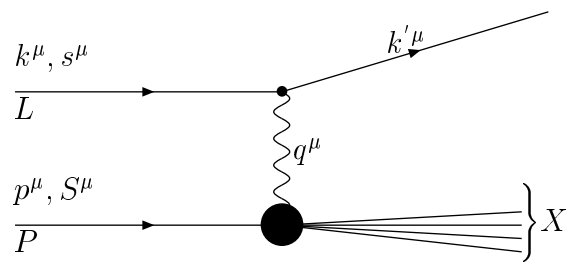

Fig. 1. Deep-inelastic scattering.

utilized naturally polarized muon beams. Consider a DIS experiment where a lepton beam with definite polarization and momentum $k^\mu = (E, \vec{k})$ scatters off a polarized proton target. This is shown in the one photon exchange diagram of Fig. 1 to leading order in the electromagnetic interaction. We work in the laboratory frame so that the proton target P has momentum $p^\mu = (M, 0)$ and polarization S^μ. The lepton L is scattered through an angle ϑ and emerges with momentum $k'^\mu = (E', \vec{k}')$. The exchanged photon carries four-momentum $q^\mu = (k - k')^\mu$. The scattering process is then characterized by the two invariants $Q^2 = -q^2$ and $\nu = p \cdot q/M$ [$\nu = (E - E')$ in the LAB frame] or, equivalently, by Q^2 and the Bjorken variable $x = \frac{Q^2}{2M\nu}$. We measure the inclusive hadronic cross section, so that hadronic final states X with the same invariant mass squared, $W^2 = (p+q)^2$, are not separated.

The spin structure experiments measure the longitudinal and transverse asymmetries

$$A_\parallel = \frac{\frac{d^2\sigma}{d\Omega dE'}^{\downarrow\Uparrow} - \frac{d^2\sigma}{d\Omega dE'}^{\uparrow\Uparrow}}{\frac{d^2\sigma}{d\Omega dE'}^{\downarrow\Uparrow} + \frac{d^2\sigma}{d\Omega dE'}^{\uparrow\Uparrow}}, \tag{1}$$

and

$$A_\perp = \frac{\frac{d^2\sigma}{d\Omega dE'}^{\downarrow\Leftarrow} - \frac{d^2\sigma}{d\Omega dE'}^{\uparrow\Leftarrow}}{\frac{d^2\sigma}{d\Omega dE'}^{\downarrow\Leftarrow} + \frac{d^2\sigma}{d\Omega dE'}^{\uparrow\Leftarrow}}\ , \tag{2}$$

where $\uparrow\downarrow$ denote the longitudinal lepton polarization and $\Uparrow\Downarrow$ ($\Leftarrow$) denote longitudinal (transverse) polarization of the target nucleon with respect to the incident beam. The polarized structure functions g_1 and g_2 are given by[17]

$$g_1(x, Q^2) \;=\; \frac{F_1(x, Q^2)}{D'} \left[A_\parallel(x, Q^2) + A_\perp(x, Q^2) \tan(\vartheta/2) \right]\ , \tag{3}$$

$$g_2(x,Q^2) \;=\; \frac{F_1(x,Q^2)}{D'}\frac{y}{2\sin\vartheta}\left[-A_{\|}(x,Q^2)\sin\vartheta + A_{\perp}(x,Q^2)\frac{E+E'\cos\vartheta}{E'}\right] \;, \quad (4)$$

where F_1 is the unpolarized structure function, $y = \nu/E$, and D' is a kinematic factor. Since the scattering angle ϑ is typically small, the parallel asymmetry primarily measures the longitudinal structure function g_1 while the transverse asymmetry is used to determine g_2.

In the naive quark-parton model, the structure function g_1 is given by the quark helicity distributions

$$g_1(x) = \frac{1}{2}\sum_q e_q^2\left[\Delta q(x) + \Delta\bar{q}(x)\right] \;, \quad (5)$$

where

$$\Delta q(x) \equiv (q^{\uparrow} - q^{\downarrow})(x) \quad (6)$$

and $q^{\uparrow}(q^{\downarrow})$ is the probability to find a quark with helicity aligned (anti-aligned) with that of a parent nucleon. The sum is over light quarks (heavy flavors contribute very little to the structure functions). The first moments of the spin-dependent parton distributions $\Delta q = \int_0^1 dx\ \Delta q(x)$ determine the fraction of the nucleon helicity carried by a parton. The total spin of the nucleon receives contributions from quarks, gluons, and orbital angular momentum,

$$\frac{1}{2}\Delta\Sigma + \Delta G + < L_z > \;\; = \frac{1}{2}. \quad (7)$$

The sum

$$\Delta\Sigma = \sum_{u,d,s}\left[\Delta q + \Delta\bar{q}\right] \quad (8)$$

is interpreted as the nucleon helicity carried by quarks, and $\Delta G \equiv \int_0^1 dx \Delta G(x)$ is the helicity carried by gluons.

In operator language, Δq_i is defined by the proton matrix element of the axial current. We write

$$2MS_\mu \Delta q_a = \;\; < p, S|\bar{q}\gamma_\mu\gamma_5\frac{\lambda^a}{2}q|p, S >, \quad (9)$$

where $a = 3, 8, 0$ denote SU(3) matrix elements. The non-singlet matrix elements also arise in the neutron and hyperon beta decays. Current algebra relates the spin-dependent (strong interaction) structure of the proton, measured in polarized deep-inelastic scattering at high energies, to the quantities needed in low-energy weak-interaction physics. The currents which measure Δq_3 and Δq_8 do

not renormalize, so these quantities are scale independent. They are determined as $\Delta q_3 = g_A = F + D$ and $\Delta q_8 = \frac{1}{\sqrt{3}}(3F - D)$ within SU(3). The axial coupling constant of the neutron beta-decay is g_A, and F and D are the antisymmetric and symmetric SU(3) couplings. One finds[18,19]

$$\Delta q_3 = (\Delta u + \Delta \bar{u}) - (\Delta d + \Delta \bar{d}) = 1.2601 \pm 0.0025, \tag{10}$$

and

$$\Delta q_8 = (\Delta u + \Delta \bar{u}) + (\Delta d + \Delta \bar{d}) - 2(\Delta s + \Delta \bar{s}) = 0.688 \pm 0.035. \tag{11}$$

Since Δq_3 and Δq_8 are determined from other experiments, by measuring the integrals $\Gamma_1^{p,n} = \int_0^1 dx\ g_1^{p,n}(x)$, we can extract the singlet "spin content" of the proton $\Delta\Sigma$ as well as individual quark contributions Δu, Δd, and Δs (we assume, again, that there is a negligible heavy quark contribution).

There are two sum rules for g_1 which can be tested in spin-dependent deep-inelastic scattering. The Bjorken sum rule[16] gives a relation for the difference between the first moment of g_1 for a proton and neutron target. In the scaling limit, it reads:

$$\int_0^1 dx\ \left(g_1^p(x) - g_1^n(x)\right) = \frac{1}{6} g_A\ . \tag{12}$$

The Bjorken sum rule was derived using current algebra before the advent of QCD and is a test of isospin symmetry. At the finite Q^2 of an experiment, one must include perturbative QCD (pQCD) Wilson coefficients:

$$\int_0^1 dx\ \left(g_1^p(x) - g_1^n(x)\right) = \frac{1}{6} g_A C_{\rm NS}(Q^2), \tag{13}$$

where the expansion for the non-singlet coefficients $C_{\rm NS}(Q^2)$ in terms of $\alpha_S(Q^2)/\pi$ is known to the third (NNNLO) order.[20,21]

The second sum rule for g_1 is the Ellis-Jaffe sum rule[22] and is a test of the Okuba, Zweig, and Iizuka (OZI) rule in the flavor singlet channel. The first moments of the spin structure functions can be expressed in terms of the SU(3) matrix elements:

$$\Gamma_1^{p,n} = \frac{C_{\rm NS}(Q^2)}{12}\left[\pm\Delta q_3 + \frac{1}{3}\Delta q_8\right] + \frac{C_{\rm S}(Q^2)}{9}\Delta\Sigma\ . \tag{14}$$

The singlet Wilson coefficients $C_{\rm S}$ have been recently computed to the third order.[23] If we assume that strange (and heavy) quarks do not play a significant role and set $\Delta s = 0$, then $\Delta\Sigma = \Delta q_8$, and the integrals Γ_1^p and Γ_1^n are determined

by the hyperon beta decays. The Ellis-Jaffe sum rule involves a model-dependent assumption that the OZI rule is obeyed, whereas the Bjorken sum rule should hold exactly in QCD. Experiments prior to E154 have found the Ellis-Jaffe sum rule to be violated by more than two standard deviations[7,9–12] and confirmed the Bjorken sum rule.[10,12,25]

1.2 Experimental Situation before E154 and E155

The first experiment on spin-dependent deep-inelastic scattering was E80 at SLAC in 1976.[5] The experiment used a polarized electron beam with energies of 9.7 and 12.9 GeV, and a polarized butanol target to measure the photon-nucleon asymmetry A_1^p. The experiment was repeated in 1980 by the same SLAC-Yale collaboration (SLAC E130)[6] with higher electron energies (16.2 and 22.7 GeV). The experiments found good agreement with the quark-parton expectations over the covered x range.

The experimental program was continued at CERN by the EMC experiment which took data in 1984–85 (Ref. 7). EMC scattered a naturally polarized μ^+ beam with energies between 120 and 200 GeV off a polarized ammonia target. The high muon energy allowed the measurement to extend to much lower x than in the original SLAC experiments. The EMC results were in good agreement with the naive quark model expectations and SLAC results for $x > 0.1$, but the data appeared to be significantly below the prediction at lower values of x. Consequently, EMC obtained for the first moment of g_1^p,

$$\Gamma_1^p(\text{EMC}) = 0.126 \pm 0.010(\text{stat.}) \pm 0.015(\text{syst.}) \tag{15}$$

at an average $Q^2 = 10$ GeV^2, about a three standard deviation disagreement with the Ellis-Jaffe prediction. Assuming $SU(3)_{\text{flavor}}$ symmetry and using Eq. (14), one can find that the total quark contribution to the proton spin is small:

$$\Delta\Sigma = 0.12 \pm 0.17. \tag{16}$$

This result came as a surprise, and the effect was even dubbed "the proton spin crisis" in the community. It has inspired a large amount of theoretical work aimed at understanding the spin structure of the proton. It has also been the genesis of a new experimental program in polarized DIS. The interest shifted towards experimental tests of the Bjorken sum rule and precision determinations of the spin structure of the nucleon.

The SLAC spin structure program restarted in the Fall of 1992 with the experiments E142[8] and E143.[9,10] Development of strained GaAs cathodes resulted in the high beam polarization of $\approx 80\%$ available to E143. The high intensity of the electron beam and the ability to flip the direction of the electron helicity on a pulse-by-pulse basis determined the statistical and systematic precision of the experiments. E142 used a high-density polarized ^{3}He target to measure the spin structure function g_1^n of the neutron, and E143 ran with polarized ammonia targets to measure the structure functions g_1^p and g_1^d of the proton and deuteron. Unlike the original SLAC experiments, the transverse asymmetry $A_\perp$ was also measured and the transverse structure function g_2 was extracted for the proton and deuteron.[24] The experiments covered the x range of $0.03 \leq x \leq 0.7$ at an average Q^2 of 2 GeV^2 (E142) and 3 GeV^2 (E143).

The program at CERN continued with the SMC experiment,[11,12] which took data with polarized deuteron targets in 1992, 1994, and 1995 (deuterated butanol was used as a target material), and with a proton target in 1993 and 1996. Like EMC, SMC used the highest energy 190 GeV muon beam, and the butanol target was superseded in 1996 by an ammonia target. Due to the high beam energy, the experiment reached lower values of x and higher Q^2 than the SLAC experiments. The measurements covered the x range of $0.003 \leq x \leq 0.7$ at an average Q^2 of 10 GeV^2. However, the muon intensity was low, and statistics limit the precision of the SMC measurements.

A new spin structure program was started recently at DESY. The HERMES experiment operates in the HERA storage ring utilizing the 27 GeV positrons (electrons) and polarized internal gas targets. The first inclusive results from the 1995 run with a ^{3}He target have been published.[13]

The summary of the data available prior to E154 is given in Table 1 and Figs. 2 and 3. The consistency of the data taken in different experiments and at different kinematics is outstanding. Not only are the tests of sum rules possible, but information about the shape of the structure functions and the underlying parton distributions has begun to emerge.

Barring difficulties with the low-x extrapolation and the Q^2 evolution of the structure functions, the values of the moments in Table 1 can be used to test the Bjorken sum rule and extract the total quark contribution to the proton helicity

Table 1. Values of the first moments of g_1^p, g_1^n, and g_1^d reported by experiments at SLAC and CERN.

Experiment	Target	Q^2 (GeV^2)	$\Gamma_1 \pm$ stat. $\pm$ syst.	Ref.
CERN EMC	p	10	$0.126 \pm 0.010 \pm 0.015$	[7]
CERN SMC	p	10	$0.136 \pm 0.011 \pm 0.011$	[11]
CERN SMC	d	10	$0.041 \pm 0.006 \pm 0.005$	[12]
SLAC E142	n	2	$0.031 \pm 0.006 \pm 0.009$	[8]
SLAC E143	p	3	$0.129 \pm 0.004 \pm 0.009$	[9]
SLAC E143	d	3	$0.042 \pm 0.003 \pm 0.004$	[10]

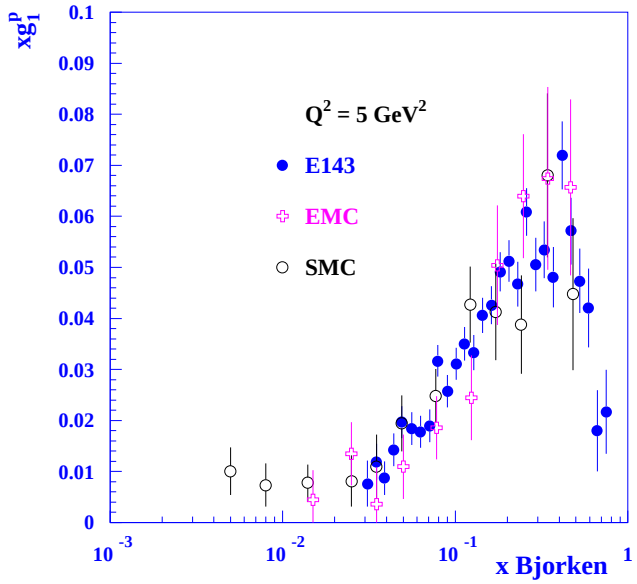

Fig. 2. World data on $xg_1^p(x)$.

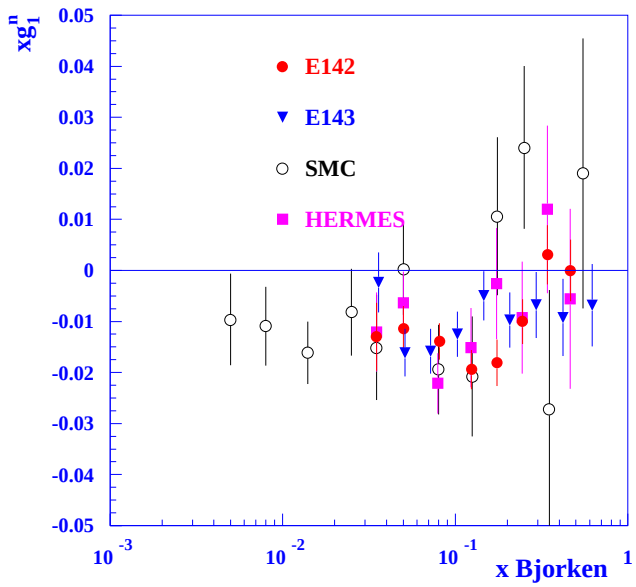

Fig. 3. World data on $xg_1^n(x)$.

$\Delta\Sigma$. Ellis and Karliner[25] performed a global fit to the data and obtained

$$\int_0^1 dx \left[g_1^p(x,Q^2) - g_1^n(x,Q^2)\right] = 0.164 \pm 0.011 \tag{17}$$

at $Q^2 = 3$ GeV^2, in perfect agreement with the prediction. For the quark helicity contributions, Ellis and Karliner obtained[25]

$$\begin{aligned} \Delta u + \Delta\bar{u} &= 0.82 \pm 0.03 \\ \Delta d + \Delta\bar{d} &= -0.44 \pm 0.03 \\ \Delta s + \Delta\bar{s} &= -0.11 \pm 0.03 \end{aligned} \tag{18}$$

and

$$\Delta\Sigma = 0.27 \pm 0.04. \tag{19}$$

One has to keep in mind, of course, that the theoretical errors associated with the low x extrapolation, Q^2 dependence of asymmetries, higher twist effects, etc., have not been included in Eqs. (18) and (19).

Several pQCD fits to the polarized deep-inelastic data have been made in the leading[26–29] and next-to-leading[30–32] orders in α_S. The first information on the polarized parton distributions has become available.

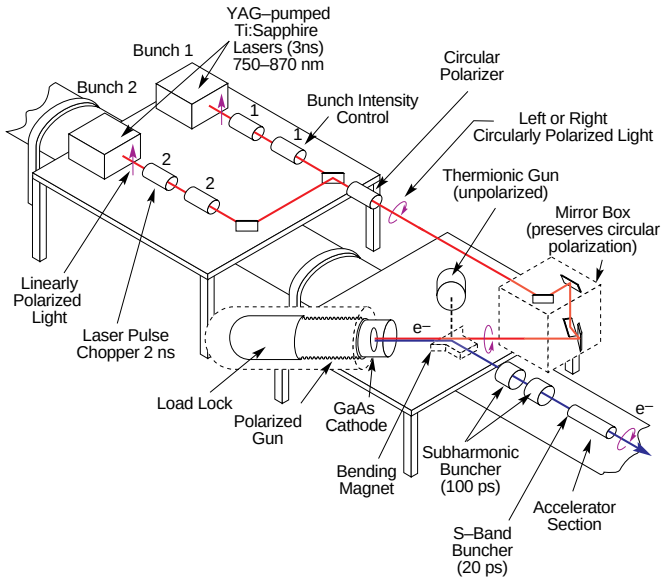

Fig. 4. A schematic of the polarized source at SLAC. The setup shown is for the SLC operation. The E154 setup was very similar, with one of the lasers changed to a flashlamp-pumped Ti:sapphire.

2 SLAC E154 and E155

2.1 Polarized Electron Beam

One of the main components of the SLAC experimental setup was the high-intensity, 48.3 GeV polarized electron beam. Recent advances in photocathode technology provided for high polarization, an important factor in achieving high statistical precision.

The polarized electrons were produced by photoemission from a strained GaAs photocathode.[33,34] The photocathode was illuminated by a flashlamp-pumped Ti:sapphire laser that produced 200–350 ns long pulses at a wavelength of 850 nm with a 120 Hz frequency. A schematic of the polarized source is presented in Fig. 4. The laser light was polarized with a linear polarizer and a combination of two Pockels cells. The helicity of the light (and hence the direction of electron polarization) was changed pseudo-randomly on a pulse-to-pulse basis by changing the voltage on one of the Pockels cells. Possible false asymmetries due to slow

changes in spectrometer acceptance and detector efficiencies were thus reduced to a negligible level. Typical beam polarizations of $\approx 80\%$ were achieved.

The longitudinally polarized electrons were accelerated in the linac to 48.3 GeV and directed into End Station A (ESA). The beam polarization was measured periodically by a Møller polarimeter. The polarimeter consisted of a polarized iron foil target, a momentum-analyzing magnet, and a finely-segmented detector. In addition to the single-arm polarimeter used in E154,[35] a double-arm polarimeter was employed for E155.[36] Both detectors gave consistent results, and the typical precision of the measurement was $\approx 3\%$.

2.2 Polarized Targets

The polarized ^{3}He target[37] used in E154 was one of the major factors that determined the success of the experiment. It was very similar to the polarized target used in E142.[38] The target was a two-chambered 30-cm long glass cell containing ^{3}He at densities of 2.6×10^{20} atoms/cm^3. The ^{3}He nuclei were polarized in the top (pumping) chamber via spin exchange collisions with optically pumped Rubidium atoms.[39] The polarized ^{3}He gas then diffused to the bottom (target) cell. The polarization axis was determined by an external magnetic field of $\approx$ 20 G. The schematic of the ^{3}He polarized target is shown in Fig. 5.

The target polarization was measured in the target cell by Adiabatic Fast Passage (AFP) NMR[40] and, independently, in the pumping cell by the Electron Paramagnetic Resonance (EPR) technique.[41] Both methods produced consistent results with a relative uncertainty in the measurement of polarization of 5%. Target polarizations of nearly 50% were achieved, with an average polarization of 38%.

The ratio of the scattering rate from polarized ^{3}He to the total rate (the *dilution factor*) was increased in E154 by almost a factor of two compared to E142. The end windows of the target cell were made concave (see Fig. 5) and thinner. The dilution factor was calculated using existing measurements of the unpolarized structure function[42] $F_2(x, Q^2)$ and a fit to the data on $R(x, Q^2)$, the ratio of longitudinal to transverse photoabsorption cross sections from SLAC.[43] The dilution factor was also measured by comparing rates from the polarized target to rates from a dummy cell with variable gas pressure. On average, the dilution factor was found to be 0.55 ± 0.03.

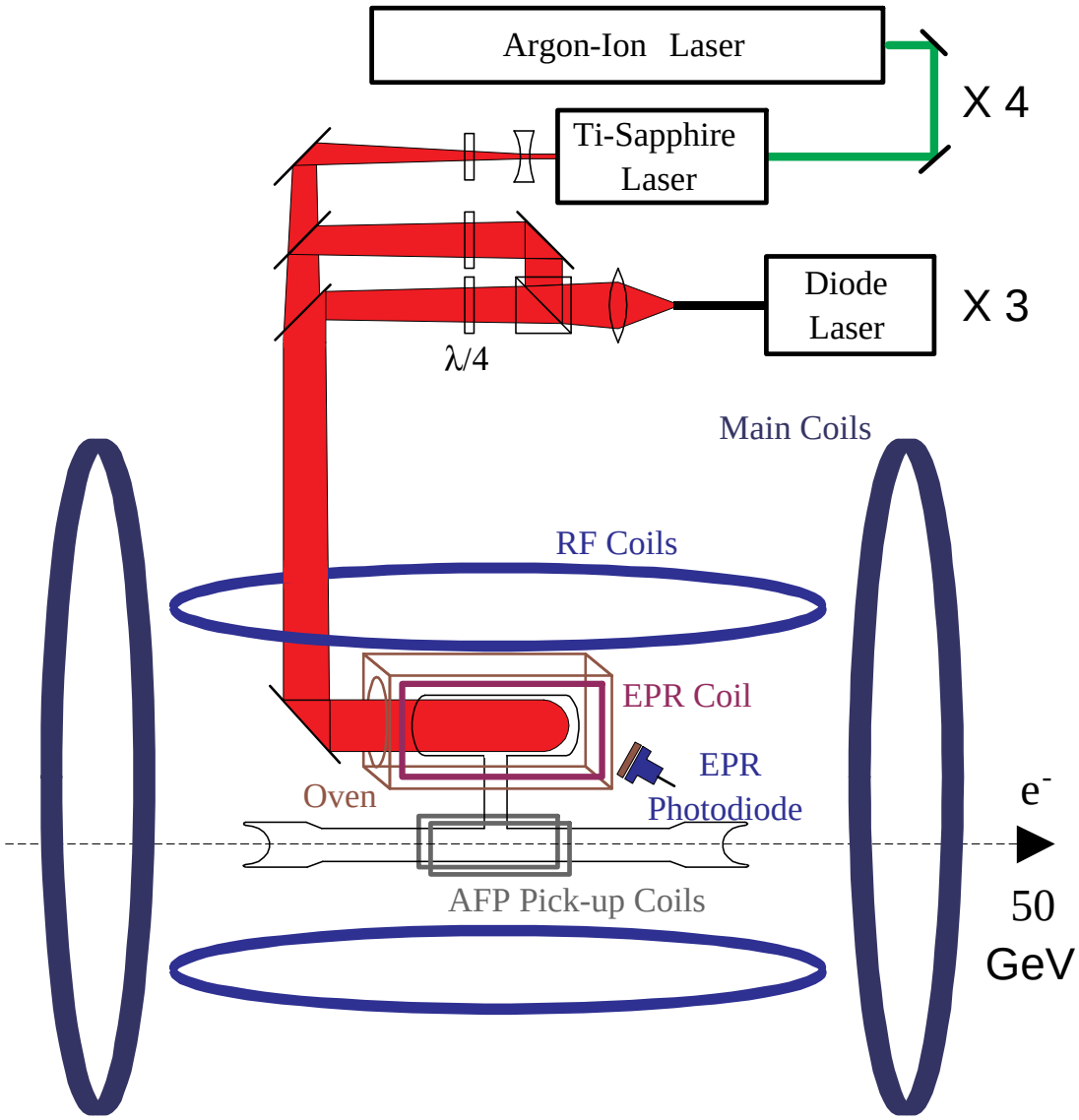

Fig. 5. The schematic of the E154 polarized target setup.

The experiment E155 used cryogenic proton and deuteron targets which were polarized using a technique of Dynamical Nuclear Polarization (DNP).[44] Solid beads of ammonia (NH_3) and LiD were frozen in a bath of liquid helium to ≈ 1 K and polarized in the magnetic field of 5 T. The polarization was measured using the NMR technique, with a relative precision of $\approx 4\%$. Polarizations of up to 95% (25%) were achieved for NH_3 (LiD) with an in-beam average polarization of 83% (23%). The dilution factor for protons in NH_3 was 0.16 on average. The dilution factor for deuteron in LiD was ≈ 0.5, more than a factor of two larger than in the ND_3 target used in E143. The schematic of the cryogenic targets is shown in Fig. 6.

2.3 Magnetic Spectrometers

Scattered electrons were detected simultaneously in two independent large acceptance magnetic spectrometers centered around 2.75° and 5.5° relative to the beam line.* The 48.3 GeV beam, combined with the choice of angles, allowed measurements in the kinematic range $0.014 \leq x \leq 0.8$ and 1 GeV$^2 \leq Q^2 \leq 17$ GeV^2. The 2.75° spectrometer covers a momentum range from 10 to 44 GeV, and the 5.5° spectrometer covers a momentum range from 10 to 39 GeV.

A system of two independent "closed-geometry" magnetic spectrometers with two dipoles bending the scattered electrons in the opposite directions has several advantages. First, the neutral background is highly suppressed with the so-called *"double-bounce"* geometry,[45] which prevents neutral particles from reaching the detectors without bouncing at least twice off the magnets and collimators. Second, unlike the typical open-geometry detectors used in particle physics experiments, we could choose the relative acceptances of two spectrometers in such a way that the electron rates, and therefore statistical errors, are comparable at low and high x. Two spectrometers also provide the lever arm essential for studies of the Q^2 dependence of deep-inelastic spin asymmetries. The schematic plan of the spectrometers is shown in Fig. 7.

Each spectrometer was equipped with a pair of threshold Cherenkov detectors operating with nitrogen at a pressure of 1.5 (2) psi in the 2.75° (5.5°) spectrometer. The pressure corresponds to the pion threshold of 19 (16) GeV. The Cherenkov

*A third spectrometer centered at 10.5° to the beam line was built for E155. Results from this spectrometer are not yet available.

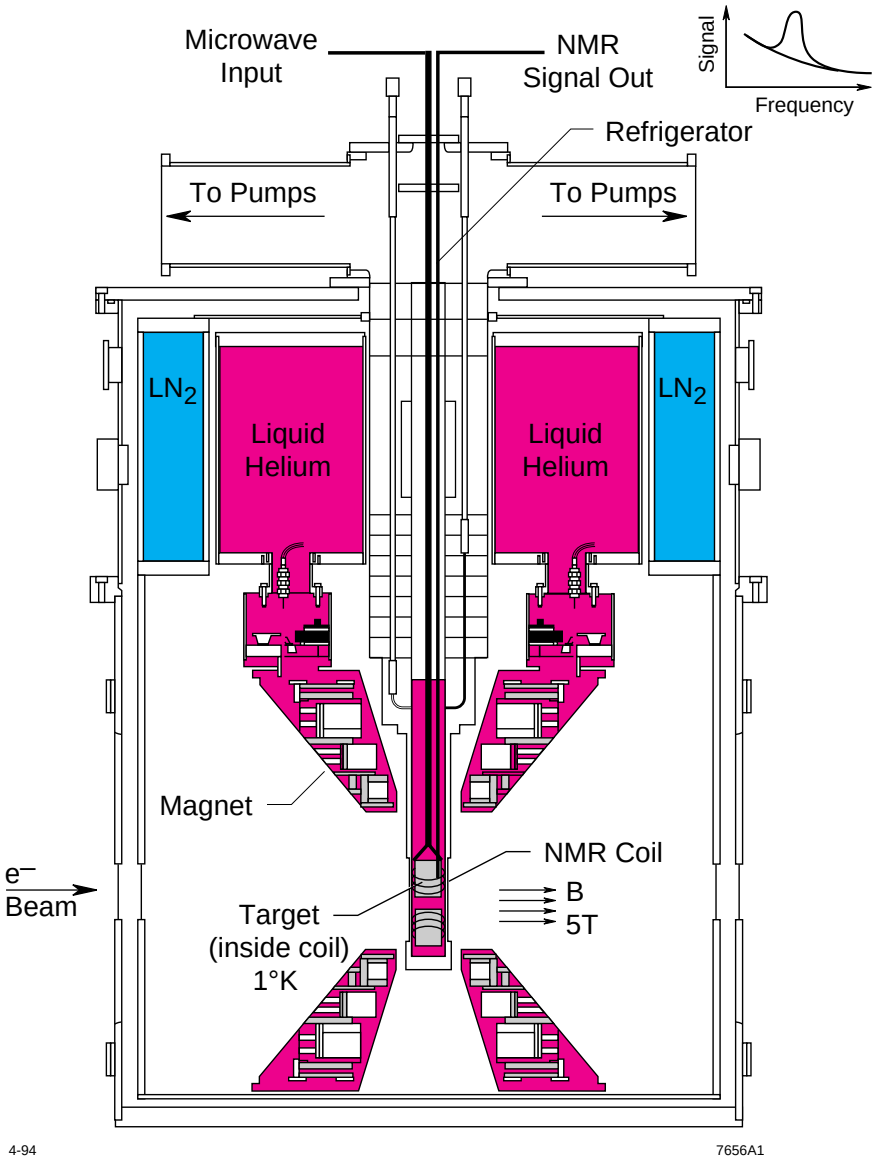

Fig. 6. The schematic of the E155 polarized target setup.

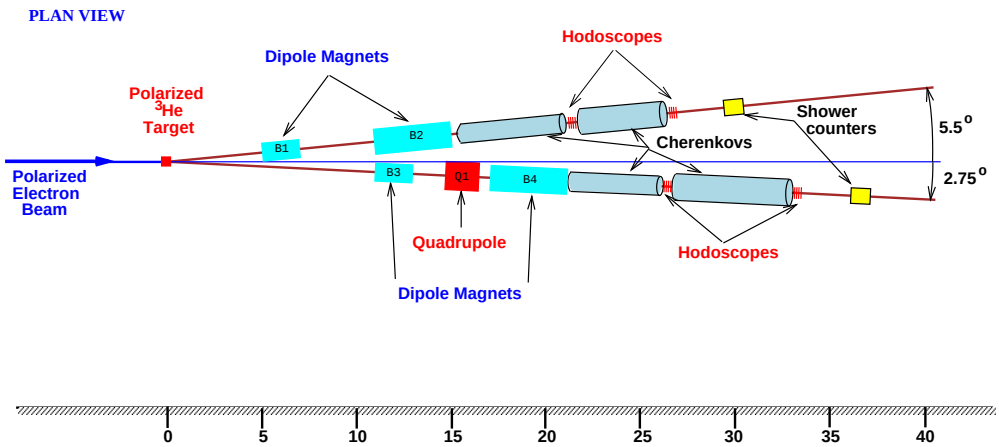

Fig. 7. Schematic plan of the E154/E155 spectrometers.

photons were focused by a spherical mirror on a single five-inch diameter phototube. A typical electron event produced on average 4.5–6.5 photoelectrons in each counter. The phototube pulses were digitized by a Flash ADC that recorded the pulse height in 1 ns time slices over the length of the beam spill.

Ten (eight) planes of hodoscopes were used for tracking in the 2.75° (5.5°) spectrometer. The tracking momentum resolution ranged from 2% at low momentum to 4% at high momentum, while the scattering angle was determined to be better than 1 mrad.[46] This resolution was sufficient for determining the kinematics of an event. Multihit TDCs provided 0.5 ns (1 ns) time resolution in the 2.75° (5.5°) spectrometer, which eliminated combinatorial background from random background hits.

A total absorption lead glass calorimeter[47] in each spectrometer consisted of 200 blocks in fly's eye configuration and provided an energy resolution of $3\% + (8/\sqrt{E(\mathrm{GeV})})$. Calorimeter phototubes were read out by ADCs and multihit TDCs. Phototubes in the high-rate region of the 2.75° spectrometer had three TDC channels with different discriminator thresholds to help reconstruct overlapping clusters.

3 Results from E154

The experiment E154 collected about 100 million deep-inelastic events in October and November of 1995. The data were taken at the beam energy of 48.3 GeV and at three nominal beam currents: 3×10^{10}, 5×10^{10}, and 9×10^{10} electrons per pulse. Nine polarized target cells and four reference cells were used through the course of the experiment. The typical electron rate was 0.5 electrons per pulse in the 2.75° spectrometer, and varied from 0.07 to 0.2 electrons per pulse in the 5.5° spectrometer. The data set included asymmetry data (in parallel and perpendicular target polarization configurations), reference cell runs to determine the dilution factor, runs with the magnet polarity reversed to measure the charge symmetric backgrounds, and miscellaneous calibration and test runs.

3.1 Data Analysis

For every beam pulse, the tracks were reconstructed using the time and spatial information from the shower counter and two sets of hodoscopes. The tracking efficiency was measured to be above 90% for typical running conditions.[46] The tracks were selected as electron candidates if they passed a low threshold cut in both Cherenkov detectors, which typically corresponded to 1.5–2.5 photoelectrons. The hadronic background was further reduced by cuts on the ratio of total energy deposited in the shower counter to the track momentum, $E/p > 0.8$, and on the lateral shower profile.

The charged hadron contamination to the electron sample was measured to be $3\% \pm 2\%$ in the lowest bin in Bjorken x and decreased rapidly at higher values of x. The helicity asymmetry of the inclusive pion sample was found to be $\approx 1/3$ of the size of the DIS asymmetry. On the other hand, contamination to the DIS sample from the charge-symmetric processes was found to be significant, $\approx 15\%$ for the lowest momenta in the 2.75° spectrometer. This contamination decreased quickly at higher values of momentum. The asymmetry of the charge-symmetric sample was found to be consistent with zero; however, the statistical error in this number was the biggest contribution to the systematic uncertainty at low x.

The experimental asymmetries $A_{\parallel}$ and $A_{\perp}$ were corrected for the hadronic and charge-symmetric backgrounds, dilution factor, beam, and target polarization. Corrections due to rate-dependent effects were small (2%–4%), and the correction due to the parity-violating electroweak interference diagrams was at

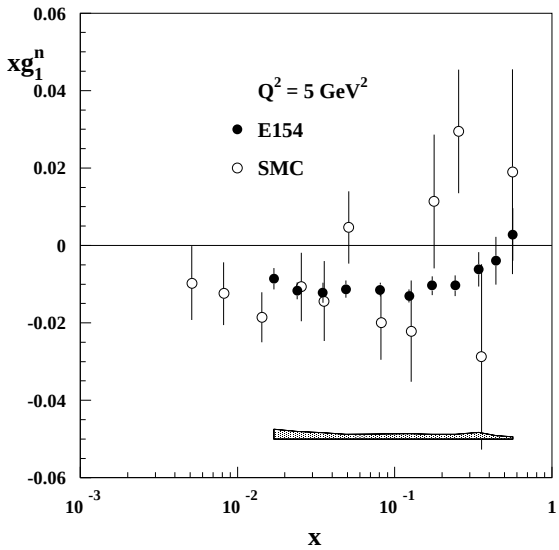

Fig. 8. A comparison of the E154 (closed circles) and SMC (open circles) data. The shaded area represents one standard deviation systematic errors.

a negligible level due to frequent reversal of both beam and target polarization directions. Finally, the radiative corrections[48,49] were applied to yield the single-photon exchange Born asymmetries and structure functions for ^{3}He.

Corrections due to the nuclear wave function[50] of the ^{3}He were applied to extract the neutron structure functions. We used the recent data on the proton spin structure functions[9,11] to evaluate contributions due to the proton polarization in ^{3}He.

3.2 Structure Function Results

The results on the spin-dependent structure function g_1^n of the neutron[14] are shown in Fig. 8, together with the results of the SMC experiment at CERN.[11,12] The data have been evaluated at a common $Q^2 = 5$ GeV^2 assuming that the ratio g_1^n/F_1^n is independent of Q^2 (see Section 4). The E154 data on g_1^n give the most precise determination of the spin-dependent structure function of the neutron to date. Our results are compared with the data from the previous SLAC experiments E142[8] and E143[9,10] in Fig. 9. The agreement among the data sets is very good. The E154 data extend the measurement of g_1^n to lower values of x compared to the previous SLAC results, and improve the precision by about a factor of two.

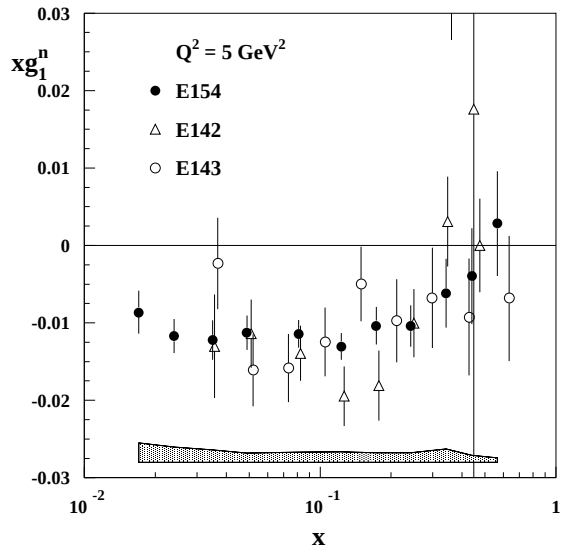

Fig. 9. The E154 results on the structure function xg_1^n (closed circles) compared to the E142 (open triangles) and E143 (open circles) data.

The most striking feature of the E154 data is the behavior of the structure function at low x. Not only does it not converge to zero as x becomes smaller, but the behavior is very divergent (Fig. 10). The data below $x = 0.1$ can be accurately fitted with a $g_1^n \sim x^{-0.8}$ power law, incompatible with a traditional Regge theory expectation[51] that g_1 is constant or convergent at low x. Such a divergent behavior makes the extrapolation to $x = 0$ problematic, as we will discuss in the following section.

3.3 Sum Rules

Over the x range covered by E154, we obtain the integral of the neutron spin-dependent structure function

$$\int_{0.0135}^{0.7} dx\ g_1^n(x) = -0.0360 \pm 0.0039 \pm 0.0045\ , \tag{20}$$

where the first uncertainty is statistical, and the second is systematic.

In order to evaluate the integral of the structure function over the full x range, the data has to be extrapolated to $x = 0$ and $x = 1$. The high-x extrapolation is straightforward. The quark-counting rules predict[52] the leading twist contribution of g_1 to fall off as $g_1 \sim (1-x)^3$ as $x \to 1$. The contribution to the integral from

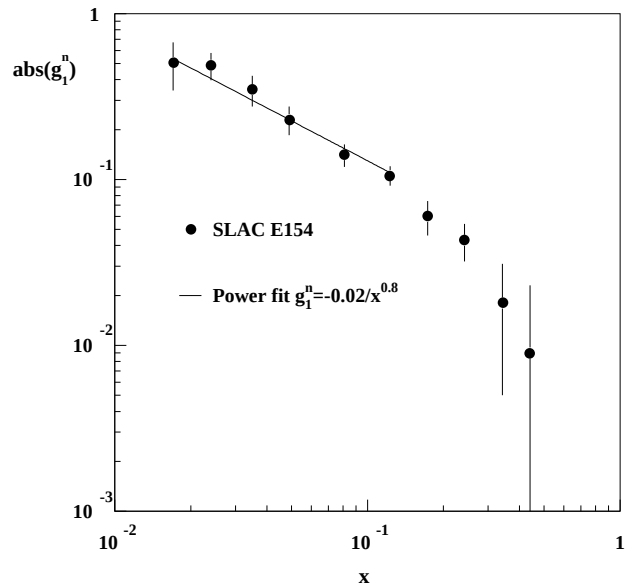

Fig. 10. The absolute value of structure function g_1^n is plotted on a log-log scale. The low-x data points of E154 are fitted with a power-law function $g_1 \sim x^{-0.8}$.

the unmeasured high x region is

$$\int_{0.7}^{1} dx\ g_1^n(x) = (0.15 \pm 0.42 \pm 0.04) \times 10^{-3}\ , \tag{21}$$

where the first uncertainty is statistical, and the second is systematic.

A much more important contribution comes from the unmeasured low-x region and it is also much more uncertain. The theoretical models vary widely in this region. The traditional approach, taken by all spin structure experiments prior to E154, was to assume the convergent Regge behavior $g_1 \sim x^{-\alpha}$, where the Regge intercept α is associated with the trajectory of the a_1 meson and is bound between -0.5 and 0 (Refs. 51 and 53). Regge theory, however, does not explicitly specify the kinematic domain (i.e., the x and Q^2 range) in which the prediction of the asymptotic behavior is applicable.

The naive Regge prediction does not describe the E154 neutron data well. Fitting the g_1^n data with a $g_1^n = const$ form (i.e., saturating the upper limit on the a_1 intercept) results in a confidence level of $0.4\ \times\ 10^{-3}$ (where all point-to-point correlations are taken into account). However, one may still fit the three lowest x points ($x < 0.04$) to a constant with a reasonable $\chi^2 = 1.7$ for two degrees of freedom. Since the Regge prediction is not very specific, we may not *a priori*

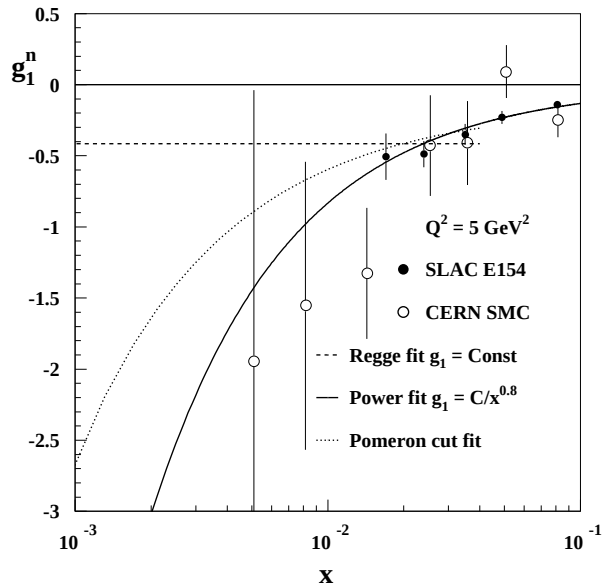

Fig. 11. Three representative fits to the low-x data of E154. Also included are the low-x data of SMC (open circles).

discard the possibility that the convergent behavior sets in at this, or an even lower value of x.

Other models of the low-x behavior have been suggested, including a singular double-Pomeron cut form,[54,55]

$$g_1 \sim \frac{1}{x \log^2 x}, \qquad x \to 0 \ , \tag{22}$$

and a model of the Pomeron based on nonperturbative gluon exchange[56] which gives a softer, but still singular behavior:

$$g_1 \sim 1 + 2 \log x, \qquad x \to 0. \tag{23}$$

Perturbative summation of contributions of the form $\alpha_S \log^2(1/x)$ yields a very divergent behavior,[57]

$$g_1^{NS} \sim \frac{1}{x^{0.4}}, \qquad g_1^S \sim \frac{1}{x^{1.01} \log^{3/2}(1/x)}, \qquad x \to 0. \tag{24}$$

Several representative fits to the E154 data are shown in Fig. 11.

The spread of the possible contributions from the low-x region is very big even for moderately convergent models. Relatively large values of the neutron spin

structure function g_1^n at low x question the validity of a naive application of the Regge theory to the present-day spin structure experiments. It would seem unnatural if the situation were any better with the proton and deuteron structure functions; most likely, the experiments have not yet reached the kinematic range and precision required to see the true asymptotic behavior at low x. A possible interpretation of our data is that the neutron structure function (or at least its derivative with respect to x) is dominated by the sea quark and gluon contributions, which in fact could produce very divergent behavior at low x.[57] We will return to this question in the following section.

4 Next-to-Leading Order Analysis of the Data

Recent progress in both experiment and theory has made polarized DIS into a powerful tool for QCD phenomenology. On the theoretical side, a full calculation of the Next-to-Leading Order (NLO) spin-dependent anomalous dimensions has recently been completed.[58] This provides for a perturbative QCD analysis of polarized DIS analogous to the treatment of the unpolarized data.[59–61] At the same time, improvement in the precision of the experimental data and increased kinematic coverage has made such an analysis increasingly more meaningful.

An apparent disagreement of the E154 data at low x with a traditional Regge behavior could be attributed to a large contribution to g_1^n from the singlet quark distribution. This implies the importance of the dynamics of polarized quark and gluon distributions, and in particular, a possibly sizable Q^2 dependence of the experimental asymmetries. Several analyses[30–32] had been done before the E154 results became available. We have performed an NLO analysis[15] of the available world data in order to consistently take into account theoretical and experimental uncertainties and determine what additional information can be extracted from the new precision data.

4.1 Fits

We follow the ansatz of Ref. 30 and parameterize the polarized parton distribution at the low initial scale $Q_0^2 = 0.34$ GeV^2 as follows:[15]

$$\Delta f(x, Q_0^2) = A_f x^{\alpha_f} (1-x)^{\beta_f} f(x, Q_0^2) \,, \tag{25}$$

where $\Delta f = \Delta u_V$, Δd_V, $\Delta\bar{Q}$, ΔG are the polarized valence, sea, and gluon distributions, and $f(x, Q_0^2)$ are the unpolarized parton distributions from Ref. 60.

We require positivity,

$$|\Delta f(x)| \leq f(x), \tag{26}$$

at all scales $Q^2 \geq Q_0^2$, which leads to the constraints $\alpha_f \geq 0$ and $\beta_f \geq 0$. In addition, we assume the helicity retention properties of the parton distributions[52] that constrain $\beta_f = 0$. We have checked that the data are consistent with this assumption. The remaining eight coefficients were determined by fitting the available data on the spin-dependent structure functions $g_1^{p,n,d}$ of the proton,[7,9,11,62] neutron,[8,13,14] and deuteron[10,12,62] with $Q^2 > 1$ GeV^2. We used either the results for g_1 or determined the structure functions at the experimental values of Q^2 using the results for g_1/F_1. The unpolarized structure function F_1 was obtained from the recent parameterization of $F_2(x, Q^2)$ from NMC[42] and the fit to the data on $R(x, Q^2)$, the ratio of longitudinal to transverse photoabsorption cross sections, from SLAC.[43]

One of the primary uncertainties in the interpretation of the deep-inelastic scattering data is the relative freedom in defining the hard scattering cross sections and the singlet quark density $\Delta\Sigma$ at the next-to-leading order, known as the factorization scheme dependence.[63,64] Additional uncertainty comes from the lack of knowledge of the higher-order corrections, and is conventionally referred to as a *renormalization scale* dependence. Several prescriptions for setting the renormalization scale exist.[66] We have choosen Q^2 to be the renormalization scale and estimate the uncertainty by varying the scale. In order to demonstrate the effects of the factorization scheme dependence, we perform our calculations[15] in both the $\overline{\text{MS}}$ scheme of t'Hooft and Veltman[65] and the Adler–Bardeen (AB) scheme,[31] in which $\Delta\Sigma$ is scale-independent.[67]

The biggest source of theoretical uncertainty was the error on the value of α_S. We estimated it by repeating the fits with $\alpha_S(M_Z^2)$ varied in the range allowed by the unpolarized DIS experiments[18] $\alpha_S(M_Z^2) = 0.108 - 0.116$, the scale uncertainty being the biggest contribution to this uncertainty. We also varied current quark masses in the range $m_c = 1 - 2$ GeV and $m_b = 4 - 5$ GeV. The sensitivity to the shape of the initial distributions and the value of the starting scale Q_0^2 was estimated by repeating the fit with initial unpolarized distributions taken from Ref. 59 at $Q_0^2 = 1$ GeV^2; the first moments were found to be stable within the statistical uncertainties. The effect of the $SU(3)_{\text{flavor}}$ breaking was estimated by

varying the parameter λ_s from 1 to 0. Possible higher twist effects were neglected since they are expected to drop[68] as $1/W^2$ and the cut $W^2 > 4$ GeV^2 has been applied to all the data, with the majority of them exceeding $W^2 > 8$ GeV^2.

4.2 Results and Discussion

Results for the structure functions of the proton and neutron g_1^p and g_1^n at 5 GeV^2 are compared to the experimental data in Fig. 12. The fits are excellent despite a small number of free parameters. We find that at the initial scale $Q^2 = 0.34$ GeV^2 the low-x behavior of the distributions is consistent with the Regge theory prediction[51] $g_1 \sim const$. However, Regge theory in the past has been applied at the $Q^2 \sim$2–10 GeV^2 of the experiments. This procedure clearly cannot be applied to the E154 neutron data for $0.014 < x < 0.1$, and is incompatible with the pQCD predictions.[57,69]

It is interesting to note that the proton structure function is predicted to cross zero between $x = 0.001$ and $x = 0.01$ (at $Q^2 = 5$ GeV^2). This is due to the sea and gluon contributions that start to dominate at sufficiently low x. Since the neutron structure function g_1^n is large and negative, the deuteron structure function g_1^d is expected to cross zero near $x = 0.01$. The contributions from the valence quarks and sea quarks and gluons to the neutron spin structure function at $Q^2 = 5$ GeV^2 are shown in Fig. 13. One can see that the sea and gluon contributions are larger than the valence contributions at $x \approx 10^{-3}$. Although the sea contributions to g_1^n are relatively modest in the E154 data range $x > 0.01$, the strong x dependence $g_1^n \sim x^{-0.8}$ observed by E154 below $x = 0.1$ is largely due to the sea and gluon contributions. An observation of a negative value of g_1^p at lower x and higher Q^2 would provide direct evidence of a polarized sea.

For the first moments of the polarized gluon distribution ΔG and the total quark helicity $\Delta\Sigma$ we obtain in the $\overline{\mathrm{MS}}$ scheme

$$\begin{aligned} \Delta G &= 1.8^{+0.6}_{-0.7}(\mathrm{stat.})^{+0.4}_{-0.5}(\mathrm{syst.})^{+0.1}_{-0.6}(\mathrm{theory}), \\ \Delta\Sigma &= 0.20^{+0.05}_{-0.06}(\mathrm{stat.})^{+0.04}_{-0.05}(\mathrm{syst.})^{+0.01}_{-0.01}(\mathrm{theory})\ . \end{aligned} \tag{27}$$

The integral of the polarized gluon distribution is positive, but the value is still poorly constrained. Note that the statistical and systematic errors are comparable. The theoretical error, dominated by the uncertainty on α_S, is also quite large. It could potentially be reduced if a simultaneous analysis of the unpolarized

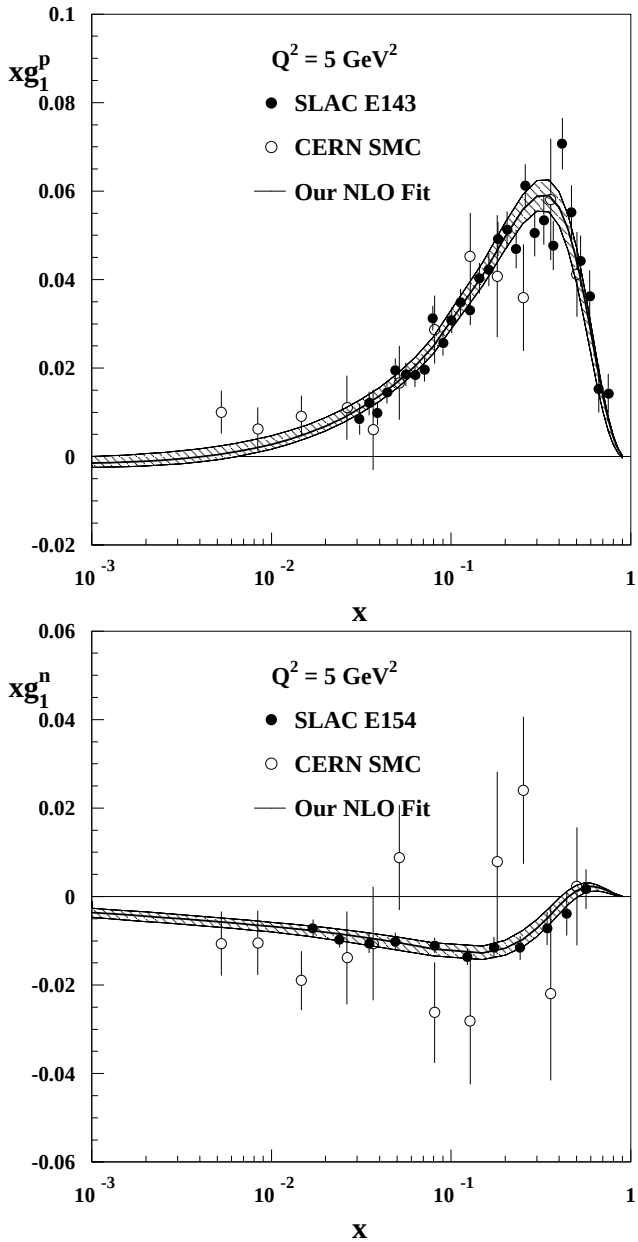

Fig. 12. The structure functions (top) xg_1^p and (bottom) xg_1^n at $Q^2 = 5$ GeV^2. E143, SMC, and E154 data have been evolved to $Q^2 = 5$ GeV^2 using a procedure described in the text. The result of the $\overline{\text{MS}}$ fit is shown by the solid line and the hatched area represents the total error of the fit.

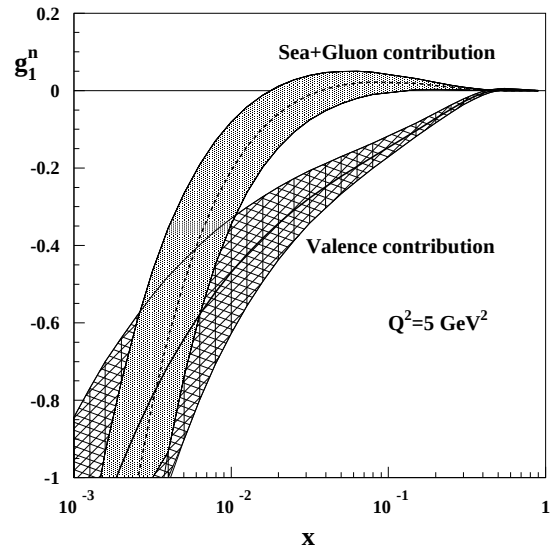

Fig. 13. The contributions to the structure function g_1^n of the neutron from the valence quarks (solid line) and from the sea quarks and gluons (dashed line). The shaded and hatched areas represent the total uncertainties on each quantity.

and polarized data were performed (including α_S as one of the parameters). The uncertainties on the values of $\Delta\Sigma$ are larger than estimated by Ref. 25 due to the uncertainty in the evolution effects and low-x extrapolation embedded in our analysis. Clearly, more precision high-energy data is needed to provide a greater lever arm for constraining the evolution of the spin structure functions and determining the gluon spin density.

Using the parameterization of the parton distributions, one can obtain the polarized structure functions and evolve the experimental data points to a common $\langle Q^2 \rangle$ using the formula:

$$g_1^{\rm exp}(x_i, \langle Q^2 \rangle) = g_1^{\rm exp}(x_i, Q_i^2) - \Delta g_1^{\rm fit}(x_i, Q_i^2, \langle Q^2 \rangle) \tag{28}$$

with

$$\Delta g_1^{\rm fit}(x_i, Q_i^2, \langle Q^2 \rangle) = g_1^{\rm fit}(x_i, Q_i^2) - g_1^{\rm fit}(x_i, \langle Q^2 \rangle), \tag{29}$$

where $g_1^{\rm exp}(x_i, Q_i^2)$ is the structure function measured at the experimental kinematics, and $g_1^{\rm fit}$ is the fitted value. Using this procedure, we obtain the integral of the neutron structure function in the measured range,

$$\int_{0.0135}^{0.7} dx\ g_1^n(x) = -0.035 \pm 0.003 \pm 0.005 \pm 0.001, \tag{30}$$

where the first error is statistical, the second is systematic, and the third is due to the uncertainty in the evolution. Moreover, we can use the NLO fits to calculate the contributions to the full integral from the unmeasured high-x, and more importantly, low-x regions. We use the E154 data to obtain the neutron integral

$$\Gamma_1^n = -0.058 \pm 0.004 \text{ (stat.)} \pm 0.007 \text{ (syst.)} \pm 0.007 \text{ (evol.)}. \tag{31}$$

Combining the E154 neutron result with the proton data from E143,[9] we determine the Bjorken integral

$$\Gamma_1^{p-n}(5 \text{ GeV}^2) = \int_0^1 dx \; (g_1^p - g_1^n) = 0.171 \pm 0.005 \pm 0.010 \pm 0.006, \tag{32}$$

where the first error is statistical, the second is systematic, and the third is due to the uncertainty in the evolution and low x extrapolation. This value is in good agreement with the $O(\alpha_S^3)$ prediction[21] 0.188 evaluated with $\alpha_S(M_Z^2) = 0.109$, and it also agrees very well with the world average

$$\Gamma_1^{p-n} = 0.168^{+0.005}_{-0.004}(\text{stat.})^{+0.008}_{-0.007}(\text{syst.})^{+0.007}_{-0.001}(\text{theory}) \tag{33}$$

obtained by direct integration of the parton densities. The result is fairly insensitive to the details of the low-x extrapolation which is well constrained by the data. The low x behavior in the non-singlet polarized sector is also relatively insensitive to the higher-order corrections.[70]

5 Preliminary Results from E155

SLAC experiment E155 took data on the spin structure functions of the proton and deuteron in early 1997. The preliminary results on g_1^p are shown in Fig. 14. The precision of the measurement is significantly improved over the previous experiments. A similar improvement is expected for the deuteron structure function g_1^d when the results become available. An extension of the E155 run is scheduled for early 1999 to measure the transverse structure functions g_2^p and g_2^d.

6 Conclusion and Outlook

The recent experiments at SLAC have improved the determination of the spin-dependent structure functions. The increased beam energy allowed us to extend

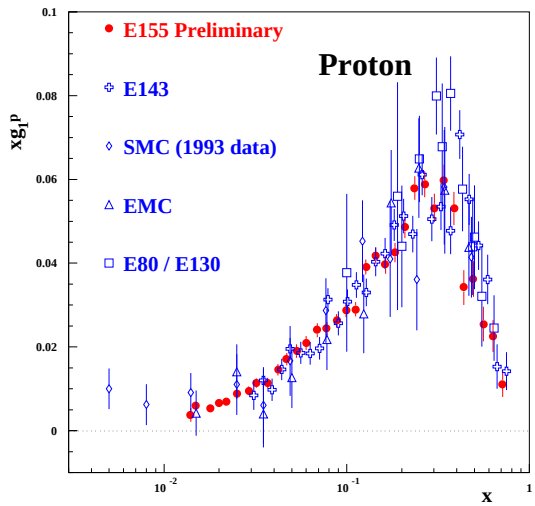

Fig. 14. The preliminary results from E155 compared to the world data on xg_1^p.

the measurements to lower values of Bjorken variable x and to increase the four-momentum transfer Q^2, providing for a possibility to constrain the evolution of the polarized parton distributions. Thus, not only can the information about the quark contribution to the structure functions be obtained from the present data, but also first constraints on the gluon helicity distribution are emerging.

At the same time, the data presented us with some surprises. We have observed relatively large values of g_1^n at low x, and the behavior of the structure function seems to be quite divergent. This apparently disagrees with predictions of the conventional Regge theory, and poses certain problems for extrapolating the data to $x = 0$ in order to evaluate the first moment of g_1^n and test the Ellis-Jaffe sum rule. While such a behavior is qualitatively understood in perturbative QCD, firm quantitative predictions are not yet available.

In order to reduce the ambiguity in the interpretation of the results, we have performed a Next-to-Leading Order QCD analysis of the world data on polarized deep-inelastic scattering. We find that the data constrain the first moments of the polarized valence quark distributions; the polarized gluon and sea quark distributions can only be qualitatively constrained. Assuming the validity of the NLO approximation, we determine the first moments of the spin-dependent structure functions of the proton and neutron, and find agreement with the Bjorken sum

rule. However, for an unambiguous determination of the total quark helicity and the polarized gluon distribution, data at higher energies are needed.

In the near future, the results from E155 on the polarized structure function g_1^d of the deuteron will be available. The spin structure program will continue into the next century with the semi-inclusive data from HERMES, greater kinematic coverage at the polarized HERA, and direct measurements of the gluon and sea helicity contributions at CERN, HERA, and RHIC. Spin-dependent deep-inelastic scattering is sure to provide us with more exciting insights into the structure of the nucleon.

References

[1] E. D. Bloom *et al.*, Phys. Rev. Lett. **23**, 930 (1969);
M. Breidenbach *et al.*, Phys. Rev. Lett. **23**, 935 (1969).

[2] R. P. Feynman, Phys. Rev. Lett. **23**, 1415 (1969).

[3] J. D. Bjorken, Phys. Rev. D **1**, 1376 (1970).

[4] J. D. Bjorken and E. A. Paschos, Phys. Rev. **185**, 1975 (1969).

[5] The E80 Collaboration, M. J. Alguard *et al.*, Phys. Rev. Lett. **37**, 1258 (1976); Phys. Rev. Lett. **37**, 1261 (1976); Phys. Rev. Lett. **41**, 70 (1978).

[6] G. Baum *et al.*, Phys. Rev. Lett. **51**, 1135 (1983).

[7] The EMC Collaboration, J. Ashman *et al.*, Phys. Lett. B **206**, 364 (1988);
Nucl. Phys. B **328**, 1 (1990);
V. Hughes *et al.*, Phys. Lett. B **212**, 511 (1988).

[8] The E142 Collaboration, P. L. Anthony *et al.*, Phys. Rev. Lett. **71**, 959 (1993); Phys. Rev. D **54**, 6620 (1996).

[9] The E143 Collaboration, K. Abe *et al.*, Phys. Rev. Lett. **74**, 346 (1995).

[10] The E143 Collaboration, K. Abe *et al.*, Phys. Rev. Lett. **75**, 25 (1995).

[11] The SMC Collaboration, D. Adams *et al.*, Phys. Lett. B **329**, 399 (1994);
Phys. Lett. D **56**, 5330 (1997);
B. Adeva *et al.*, Phys. Lett. B **412**, 414 (1997).

[12] The SMC Collaboration, B. Adeva *et al.*, Phys. Lett. B **302**, 533 (1993);
D. Adams *et al.*, Phys. Lett. B **357**, 248 (1995); Phys. Lett. B **396**, 338 (1997).

[13] The HERMES Collaboration, K. Ackerstaff *et al.*, Phys. Lett. B **404**, 383 (1997).

[14] The E154 Collaboration, K. Abe *et al.*, Phys. Rev. Lett. **79**, 26 (1997).

[15] The E154 Collaboration, K. Abe *et al.*, Phys. Lett. B **405**, 180 (1997).

[16] J. D. Bjorken, Phys. Rev. **148**, 1467 (1966); Phys. Rev. D **1**, 1376 (1970).

[17] T. Pussieux and R. Windmolders, in *Internal Spin Structure of the Nucleon*, edited by V. W. Hughes and C. Cavata (World Scientific, 1995).

[18] Review of Particle Properties, Particle Data Group (R. M. Barnett *et al.*), Phys. Rev. D **55**, 1 (1996).

[19] M. Bourquin *et al.*, Z. Phys. C **21**, 27 (1983).

[20] J. Kodaira *et al.*, Phys. Rev. D **20**, 627 (1979); Nucl. Phys. B **159**, 99 (1979).

[21] S. G. Gorishny and S. A. Larin, Phys. Lett. B **172**, 109 (1986);
S. A. Larin and J. A. M. Vermaseren, Phys. Lett. B **259**, 345 (1991).

[22] J. Ellis and R. Jaffe, Phys. Rev. D **9**, 1444 (1974).

[23] S. A. Larin, T. van Ritbergen, and J. A. M. Vermaseren, Phys. Lett. B **404**, 153 (1997).

[24] The E143 Collaboration, K. Abe *et al.*, Phys. Rev. Lett. **76**, 587 (1996).

[25] J. Ellis and M. Karliner, Phys. Lett. B **313**, 131 (1993); preprint CERN-TH/95-279, hep-ph/9510402.

[26] T. Gehrmann and W. J. Stirling, Z. Phys. C **65**, 461 (1995).

[27] G. Altarelli, P. Nason, and G. Ridolfi, Phys. Lett. B **320**, 152 (1994); *ERRATUM-ibid.* B **325**, 538 (1994).

[28] C. Bourrely *et al.*, preprint CPT-96-PE-3327, hep-ph/9604204.

[29] M. Gluck, E. Reya, and W. Vogelsang, Phys. Lett. B **359**, 201 (1995).

[30] M. Gluck *et al.*, Phys. Rev. D **53**, 4775 (1996).

[31] R. D. Ball, S. Forte, and G. Ridolfi, Phys. Lett. B **378**, 255 (1996).

[32] T. Gehrmann and W. J. Stirling, Phys. Rev. D **53**, 6100 (1996).

[33] R. Alley *et al.*, Nucl. Instrum. Methods A **365**, 1 (1995).

[34] M. Woods in *Proceedings of the 12th International Symposium on High-Energy Spin Physics*, hep-ex/9611006 (1996).

[35] H. R. Band *et al.*, Nucl. Instrum. Methods A **400**, 24 (1997).

[36] A. Feltham *et al.*, submitted to *Nucl. Instrum. Methods.*

[37] M. V. Romalis, Ph. D. thesis, Princeton University (1997).

[38] H. Middleton, Ph. D. thesis, Princeton University (1994).

[39] W. Happer, Rev. Mod. Phys. **44**, 169 (1972).

[40] A. Abragam, *Principles of Nuclear Magnetism* (Oxford University Press, New York, 1961).

[41] N. R. Newbury *et al.*, Phys. Rev. A **48**, 558 (1993);
A. S. Barton *et al.*, Phys. Rev. A **49**, 2766 (1994).

[42] M. Arneodo *et al.*, Phys. Lett. B **364**, 107 (1995).

[43] L. W. Whitlow *et al.*, Phys. Lett. B **250**, 193 (1990);
S. Dasu *et al.*, Phys. Rev. D **49**, 5641 (1994).

[44] M. Borghini, Phys. Rev. Lett. **20**, 419 (1968).

[45] G. G. Petratos *et al.*, preprint SLAC-PUB-5678 (1991).

[46] Yu. G. Kolomensky, Ph.D. Thesis, University of Massachusetts; report SLAC-R-0503 (1997).

[47] H. Borel *et al.*, IEEE Trans. on Nucl. Sci. **Vol. 42**, No. 4, 529 (1995).

[48] D. Y. Bardin and N. M. Shumeiko, Nucl. Phys. B **127**, 242 (1977);
I. V. Akushevich and N. M. Shumeiko, J. Phys. G **20**, 513 (1994).

[49] L. W. Mo and Y. S. Tsai, Rev. Mod. Phys. **41**, 205 (1969);
Y. S. Tsai, SLAC-PUB-848 (1971).

[50] B. Blankleider and R. M. Woloshyn, Phys. Rev. C **29**, 538 (1984);
J. L. Friar *et al.*, Phys. Rev. C **42**, 2310 (1990);
C. Coffi degli Atti *et al.*, Phys. Rev. C **48**, 968 (1993).

[51] R. L. Heimann, Nucl. Phys. B **64**, 429 (1973).

[52] R. Blankenbecler and S. J. Brodsky, Phys. Rev. D **10**, 2973 (1974);
S. J. Brodsky, M. Burkardt, and I. Schmidt, Nucl. Phys. B **441**, 197 (1994).

[53] M. Anselmino, A. Efremov, and E. Leader, Phys. Rep. **261**, 1 (1995).

[54] J. Kuti, preprint MIT CTP #234 (1971);
J. Kuti, in *Internal Spin Structure of the Nucleon*, edited by V. W. Hughes and C. Cavata (World Scientific, 1995).

[55] F. E. Close and R. G. Roberts, Phys. Rev. Lett. **60**, 1471 (1988).

[56] S. D. Bass and P. V. Landshoff, Phys. Lett. B **336**, 537 (1994).

[57] J. Bartels, B. I. Ermolaev, and M. G. Ryskin, Z. Phys. C **70**, 273 (1996); Z. Phys. C **72**, 627 (1996).

[58] R. Mertig and W. L. van Neerven, Z. Phys. C **70**, 637 (1996); W. Vogelsang, Phys. Rev. D **54**, 2023 (1996) and references therein.

[59] A. D. Martin, R. G. Roberts, and W. J. Stirling, Phys. Lett. B **387**, 419 (1996).

[60] M. Gluck, E. Reya, and A. Vogt, Z. Phys. C **67**, 433 (1995).

[61] J. Botts *et al.*, Phys. Lett. B **304**, 159 (1993).

[62] The E143 Collaboration, K. Abe *et al.*, Phys. Lett. B **364**, 61 (1995).

[63] W. Furmanski and R. Petronzio, Z. Phys. C **11**, 293 (1982).

[64] G. T. Bodwin and J. Qiu, in *Proceedings of the Polarized Collider Workshop*, University Park, PA, (1990);
G. T. Bodwin and J. Qiu, Phys. Rev. D **41**, 2755 (1990);
J. Chyla, Phys. Rev. D **48**, 4385 (1993).

[65] G. t'Hooft and M. Veltman, Nucl. Phys. B **44**, 189 (1972).

[66] S. J. Brodsky and H. J. Lu, Phys. Rev. D **51**, 3652 (1995), and references therein.

[67] A. V. Efremov and O. V. Teryaev, JINR-E2-88-287 (1988); Phys. Lett. B **240**, 200 (1990);
G. Altarelli and G. Ross, Phys. Lett. B **212**, 391 (1988);
R. D. Carlitz, J. D. Collins, and A. H. Mueller, Phys. Lett. B **214**, 229 (1988);
R. L. Jaffe and A. Manohar, Nucl. Phys. B **337**, 509 (1990).

[68] S. J. Brodsky, P. Hoyer, A. H. Mueller, and W. Tang, Nucl. Phys. B **369**, 519 (1992).

[69] R. D. Ball, S. Forte, and G. Ridolfi, Nucl. Phys. B **444**, 287 (1996).

[70] J. Blümlein, S. Riemersma, and A. Vogt, Nucl. Phys. Proc. Suppl. C **51**, 30 (1996).